

Crosslinked ethylene butyl acrylate copolymer foams with different cellular structure interconnectivity and tortuosity: Microstructure and physical properties

E. Lopez-Gonzalez,^{1,2} S. Muñoz-Pascual,¹ C. Saiz-Arroyo,² M. A. Rodriguez-Perez¹

¹Cellular Materials Laboratory (CellMat), Condensed Matter Physics Department, University of Valladolid, Paseo Belén 7 47011, Valladolid, Spain

²CellMat Technologies S.L., Paseo de Belen 9-A (CTTA Building), 47011, Valladolid, Spain

Correspondence to: E. Lopez-Gonzalez (E-mail: eduardol@fmc.uva.es)

ABSTRACT: In this work, the cellular structure, physical properties, and the structure–property relationship of several novel crosslinked ethylene butyl acrylate (EBA) foams with different cellular structure interconnectivity (low tortuosity and high tortuosity) have been analyzed and compared to that of closed cell EBA foams and to that of an open-cell polyurethane foam. The results have shown that these materials present interesting properties highly dependent on the tortuosity of the cellular structure. In particular, it has been proved that reducing the tortuosity allows enhancing the acoustic absorption, the oil uptake, and the cushioning behavior. On the other hand, increasing tortuosity allows improving the impact behavior. In addition, the new open-cell materials present an enhanced damping factor for low-frequency vibrations. © 2019 Wiley Periodicals, Inc. *J. Appl. Polym. Sci.* **2019**, *136*, 48161.

KEYWORDS: oil absorption; open-cell foams; physical properties; tortuosity

Received 12 March 2019; accepted 31 May 2019

DOI: 10.1002/app.48161

INTRODUCTION

The current global policies are conducted to reduce the consumption of plastic in the coming years.¹ As a consequence, alternative routes to reduce the environmental impact must be considered due to the importance of plastic in our society. Cellular polymers, a two-phase material in which a gas is dispersed in the polymer matrix, contribute to solving this challenge because these materials allow reducing the amount of material needed to produce a specific item.^{2–4}

Cellular polymers have been introduced in numerous markets (construction, packaging, automotive, sport or acoustic insulation) in the last decades due to their excellent properties.^{5–11}

These materials can be divided into different groups considering cellular parameters such as density, anisotropy, or cells interconnectivity. Focusing on the last parameter, cellular polymers can be classified as closed cell, open-cell and cellular polymers with intermediate open-cell contents.¹² On the one hand, closed cell materials present a negligible level of interconnectivity due to the confinement of the gas inside the cells.¹³ On the other hand, the gas can move through the cellular structure in open-cell cellular polymers.¹⁴

The market of flexible open-cell cellular polymers is dominated by flexible open-cell polyurethane (PU) foams.^{15–17} PU foams present a cellular structure formed by cells mainly composed of struts, and

due to its outstanding properties, these materials are employed in a wide range of applications. Some of them are lead to improve our quality of life, for example, in comfort applications helping us to rest correctly or by acting as sound absorbers reducing the high noise levels in cities avoiding major health problems.^{18,19}

In addition, other emerging applications for open-cell flexible foams are focused on preserving the environment. Oil spill remediation is nowadays a challenging issue when crude oil is released in open waters. Not only the large but also the small, but numerous oil spills are the cause of the destruction of the environment, and they are also responsible for the death of valuable fauna and flora.^{20,21} Flexible open-cell PU foams have emerged in the last years as potential alternatives to the current methods of oil recovery.^{22–25} However, PU foams also display several drawbacks, such as the use of isocyanate as raw material or the toxicity of the fumes released in their burning, which can restrict their use in the near future. Furthermore, the poor resistance to water limits their use in oil absorption applications, since a high oil–water selectivity is required.²⁶ To overcome this critical issue, there are several studies in the literature focused on making the PU foam superhydrophobic by using surface treatments.^{27–29} However, this process raises the price of the final product and hinders industrial scalability. As a consequence, the search for potential substitutes to flexible open-cell PU foams is gaining interest.

One interesting alternative is the use of open-cell cellular polymers based on polyolefins.^{30–34} The type of cellular structure interconnectivity in crosslinked open-cell polyolefin cellular polymers is different from that of open-cell PU foams. In the case of crosslinked open-cell polyolefin materials, the gas can move through the cellular structure due to the presence of holes of different sizes in the cell walls. Both the number and the size of the holes are critical parameters to describe the cellular structure of this type of materials accurately. Thus, not only the open-cell content but also the cellular structure tortuosity is an important parameter necessary to understand the physical properties of these materials properly.^{35,36}

Typically, low-density polyethylene (LDPE) and ethylene vinyl acetate copolymer (EVA) are used as polymer matrices to produce crosslinked polyolefin foams.^{37–39} The open-cell polyolefin cellular polymers described in previous papers^{30,31} were produced by compressing foams with intermediate open-cell content generating holes in the cell walls, which typically results in materials with high tortuosities. However, as far as the authors know, there are not academic works based on the characterization and analysis of the structure–property relationship of open-cell polyolefin cellular polymers with different levels of interconnection between the cells, that is, different levels of tortuosity. In this work, novel open-cell polyolefin foams, which different levels of cells interconnections (i.e., different levels of tortuosity) have been studied.⁴⁰

In addition, it is important to comment that this is the first time that EBA polymer is used to produce crosslinked polyolefin cellular polymers. EBA was chosen owing to its excellent properties regarding flexibility, which makes these copolymers excellent candidates to replace open-cell PU materials.

EXPERIMENTAL

Materials

Several EBA foams with different cellular structure interconnectivity and tortuosity were provided by CellMat Technologies S.L. (Valladolid, Spain). The materials were produced using a two-step compression molding process.⁴⁰ EBA EBANTIX E1715 manufactured by Repsol (Spain) with a butyl acrylate content of 17%, a density of 0.926 g cm⁻³ and a melt flow index (MFI) of 1.50 g/10 min measured at 230 °C and 2.16 kg was employed as the polymer matrix in the production of the foams.

The main differences between the cellular polymers produced for this work lie in the different levels of interconnectivity reached during the fabrication process. As a result, a foam with a low level of interconnectivity (EBA CC), a foam with an intermediate open-cell content (EBA MO) and two types of open-cell foams (EBA OC HT and EBA OC LT), with an open-cell content close to 100% were produced. The main characteristics of these materials are summarized in Table I.

A commercial flexible PU foam with a density of 47 kg m⁻³ and typically used in seats in the automotive sector was used to compare its behavior with that of the EBA foams analyzed in the paper.

Typical open-cell flexible PU foams present high interconnectivity due to the absence of cell walls; the cells are mainly comprised

struts. However, both EBA OC HT and EBA OC LT foams are characterized by a different type of cellular structure interconnectivity in comparison to the open-cell PU foams. In this particular case, the interconnections between cells are produced by the presence of holes in the cell walls. The level of interconnection is related to the number and size of the holes, and thus, the tortuosity of the cellular structure. On the one hand, EBA OC HT presents small holes in the cell walls, hindering the path that the gas needs to move through the cellular structure (HT; high tortuosity). On the other hand, EBA OC LT foams are characterized by a high number and a large size of the holes (LT; low tortuosity). The holes are so large that the level of interconnectivity is similar to that of open-cell PU foams (Table I). This is explained in more detail in the section results and discussion.

As it has been mentioned in previous paragraphs, the open-cell polyolefin foams reported in previous research works were produced using the two-step compression molding process by performing an additional step to the process in which the material is compressed to create some holes in the cell walls. In our research, this procedure was followed to produce the EBA OC HT foams. This material was produced by compressing in a two-roll mill the EBA MO foam five times, fixing the distance between the roles in 80 mm. However, EBA OC LT foams were obtained directly during the foaming process without deforming the material after foaming. This was achieved by modifications in the formulation and process parameters.

Differential Scanning Calorimetry

The thermal behavior of the EBA foams was analyzed by using a Mettler DSC 822^e differential scanning calorimeter (DSC; Columbus, Ohio) previously calibrated with indium, zinc, and n-octane. The average weight of the samples used for these experiments was 1.24 ± 0.07 mg. The following temperature program was selected:

1. Heating from -40 °C to 200 °C at 10 K min⁻¹.
2. A 3-min isotherm at 200 °C.
3. Cooling from 200 °C to -40 °C at -10 K min⁻¹.
4. Heating from -40 °C to 200 °C at 10 K min⁻¹.

The crystallinity was calculated as the ratio of the melting enthalpy in the last heating step and the melting enthalpy of a 100% crystalline material (288 J g⁻¹ for 100% crystalline polyethylene). The crystallinity was estimated as the average of three measurements.

Gel Content

The gel content was measured according to ASTM D2765-16 standard procedure. Three measurements were performed for each type of material, estimating the average value. Xylene was used as the solvent. After extraction, the samples were vacuum dried overnight and then its weight was measured and compared with the initial weight of the sample before the xylene extraction.

Scanning Electron Microscopy

Scanning electron microscopy (SEM) was used to observe the differences in the cellular structure of the EBA foams with different cellular structure morphology and interconnectivity. The micrographs were taken with a Hitachi FlexSEM 1000 (Tokyo, Japan) microscope. The samples were cut with a sharp razor at room

Table I. Nomenclature, Density, Open-Cell Content, Tortuosity, Gel Content, and Crystallinity of the materials under study

Nomenclature	Density (kg m ⁻³)	Open-cell content (%)	Tortuosity	Gel content (%)	Crystallinity (%)	Cell size (μm)
EBA CC	24.3 ± 2.1	42.9 ± 3.2	- ^a	69 ± 4	15.3 ± 1.5	266.4 ± 88.9
EBA MO	20.3 ± 1.3	67.9 ± 1.0	4.3 ± 0.2	59 ± 16	14.6 ± 0.9	501.4 ± 241.4
EBA OC HT	19.7 ± 0.3	95.3 ± 0.7	4.0 ± 0.7	50 ± 9	13.6 ± 0.8	502.3 ± 255.5
EBA OC LT	20.1 ± 2.3	98.6 ± 0.3	1.9 ± 0.2	27 ± 2	14.3 ± 1.6	1339.6 ± 723.3
PU	47.2 ± 0.1	98.0 ± 0.1	1.9 ± 0.1	- ^b	- ^b	638.7 ± 222.3

^a Tests not performed because it is not possible to measure the tortuosity of this sample due to its low open-cell content.

^b The polymer matrix is a PU and therefore crystallinity was not measured.

temperature. A thin gold layer was sputtered on the fractured surface of the samples to make them conductive.

SEM was also used to estimate the cell size in 3D (ϕ) of the EBA foams. The cell size was quantified by using a tool based on the software Fiji/Image J.⁴¹

Tortuosity

The tortuosity of the EBA foams under study was estimated measuring the electrical conductivity of an ionic solution with and without the sample immersed in it.¹² The experimental setup used for the estimation of the tortuosity is schematized in Figure 1

A 0.4 M of CuSO₄·5H₂O ionic solution was used as the auxiliary liquid. Alternating current (EA-3048B Elektro-Automatik GmbH, Germany) was used in the measurements. The voltage range varied between 3 and 6 V in steps of 0.5 V. First, the electrical conductivity of the auxiliary liquid was measured without placing a sample between the electrodes, and according to Ohm's Law, the resistance was calculated (R_0). Finally, the electrical conductivity of the auxiliary liquid, including the sample between the electrodes was measured, and thus, the electrical resistance (R_f). The samples were soaked overnight to ensure the proper penetration of the solution through the cellular structure before performing the measurement. The tortuosity is given by the ratio between R_f and R_0 (1). Three measurements of each material were performed, and the average values are reported.

$$T = \frac{R_f}{R_0} \quad (1)$$

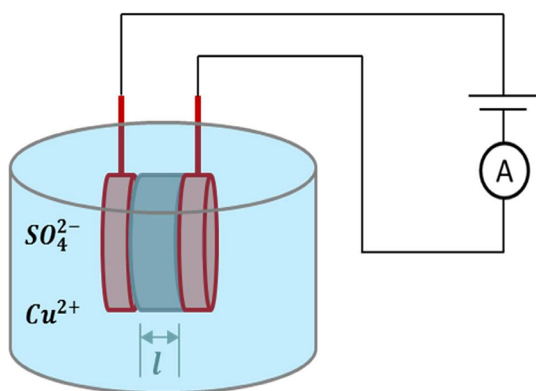


Figure 1. Scheme of the experimental setup of the tortuosity measurement. [Color figure can be viewed at wileyonlinelibrary.com]

Mechanical Properties at Low and High Strain Rates

The mechanical properties of the materials were characterized at low and high strain rates of deformation. For both tests, cubic samples of 45 × 45 × 45 mm were employed. The samples were conditioned at 23 °C for 24 h before performing the tests. Three samples of each material were tested.

The mechanical tests at low strain rates were carried out using an universal testing machine (Instron Mod. 5500R6025). The strain rate was 270 mm min⁻¹, and five load-unload cycles were performed. The maximum strain was approximately 75% for all samples independently of the type of cellular structure.

The mechanical tests at high strain rates (impact tests) were performed using an instrumented falling weight impact tester designed by CellMat Laboratory and built by the company Microtest SA (Spain).⁴² The strain rate was 1.38 × 10⁵ mm min⁻¹, approximately 500 times higher than for the tests at low strain rates.

Three following mechanical parameters were estimated from these tests: the collapse stress (MPa), the effective gas pressure (MPa), and the density of absorbed energy (J cm⁻³). The collapse stress and the effective gas pressure were calculated in the post-collapse region (between 20 and 60% strain) according to the modified model of Gent and Thomas⁴³ (2).

$$\sigma = \sigma_c + \frac{p_a(1-2\nu)\epsilon}{(1-\epsilon - \frac{\rho_f}{\rho_s})} (1-C) \quad (2)$$

where σ is the stress, σ_c is the collapse stress, $p_a(1-2\nu)(1-C)$ is the effective pressure of the gas in the sample, being p_a is the atmospheric pressure and ν is the Poisson ratio, ϵ is the strain, ρ_f is the foam density (kg m⁻³), ρ_s is the density of the solid (kg m⁻³), and its ratio (ρ_f/ρ_s) is known as the relative density (ρ_r), and finally C is the open-cell content.

The effective gas pressure accounts for the contribution of gas in the sample in the post-collapse region. As the samples are very flexible, it is intricate to measure the open-cell content using the ASTM D 2856-94 standard method in an air pycnometer because the samples deform under pressure if they have a high open-cell content. Due to this, we have used the effective gas pressure as an indirect method to measure the open-cell content. High values in the effective gas pressure indicate a lack of interconnectivity of the cellular structure, and thus, low values of open-cell content (closed cell). On the contrary, low values in the effective gas pressure mean no contribution of gas in the post-collapse region

(plateau) and as a result, high open-cell contents (open cell). The effective gas pressure can be obtained by calculating the slope of the curve σ versus $\varepsilon/(1-\varepsilon\rho_f/\rho_s)$. Based on the works of Mills *et al.*⁸ and Rodriguez-Perez *et al.*,⁴⁴ it was assumed a Poisson ratio value of 0.05 in the calculations of the effective gas pressure for the materials under study.

The density of absorbed energy is calculated as the area under the stress–strain curve. The strain limit to make the calculations was 75%. In the case of high strain rates, despite deforming the samples to values even higher than 75%, this value was also chosen as the strain to obtain the density of absorbed energy during impact.

Thermal Stability

The thermal stability was analyzed using a PerkinElmer TMA7 (Waltham) testing apparatus. The temperature program selected for the analysis was from -20 to 150 °C at 5 °C min^{-1} . Samples with cylindrical shape and diameter of 10 ± 0.1 mm and a thickness of 10 ± 0.7 mm were employed. The stress applied during testing was around 12 Pa. Three measurements were conducted for each material.

The required temperature to reduce the thickness of the foam by 10% was determined. This temperature also provides useful information about the beginning of the collapse suffered by the samples with temperature. The temperature necessary to reduce the thickness of the samples by 10% was calculated as the average of three measurements.

Dynamic Mechanical Properties

A PerkinElmer DMA 7 testing equipment with a parallel-plate mechanism was used to perform the tests. Cylindrical specimens of 10 ± 0.1 mm in diameter and 10 ± 0.8 mm in thickness were used. The measurements were carried out as a function of temperature between -40 and 150 °C at a heating rate of 5 °C min^{-1} . All materials were tested at a frequency of 1 Hz and with deformations in the linear viscoelastic regime. The modulus of the complex modulus (E^*) and $\tan \delta$ was calculated as a function of temperature. Three measurements of each material were performed.

Acoustic Properties

The acoustic behavior of the foams was characterized employing a Brüel & Kjaer (Nærum, Denmark) model 4206 impedance tube according to ASTM E1050 and ISO 10534-2. The acoustic measurements were performed in a frequency range between 500 and 6400 Hz. Cylindrical samples of 29 mm in diameter and 25 mm in thickness were used for these tests. Six measurements were performed for each material, obtaining the average value.

Oil Absorption Measurements

The oil absorption capacity of the materials under study was also analyzed using for this purpose 15 W40 commercial motor oil. Specimens with dimensions of 20 mm \times 20 mm \times 10 mm ($L \times W \times T$) were cut and weighed initially before placing them in the oil (w_0). Then, the samples were placed superficially on a beaker full of motor oil without squeezing or immersing them to favor the oil absorption. After 10 min, the specimens were extracted from the oil and were weighed again (w_1). The oil absorption capacity was measured using eq. (3):

$$\text{Oil absorption (g/g)} = \frac{(w_1 - w_0)}{w_0} \quad (3)$$

where w_0 was the initial weight of the sample before introducing in the oil and w_1 was the weight after the oil uptake. The average value of three measurements was considered for all samples.

The same methodology was followed to determine the hydrophobicity of the foams. Samples with the same dimensions as in oil absorption tests were weighed and placed superficially on a beaker full of distilled water for 10 min. The samples were extracted from the water and weighed again. Equation (3) was also used for the estimation of the water absorption.

The reusability of the materials was estimated by performing 20 compressive cycles at low strain rates (270 mm min^{-1}). The maximum strain applied was 75%. The reusability was analyzed by estimating the non-recovered deformation given by the intersection between the unload curve and the abscissa in the stress–strain curve.

RESULTS AND DISCUSSION

Structural Characterization

The main characteristics of each type of material are displayed in Table I.

As can be observed in Table I, four types of EBA foams were produced. As previously mentioned, the open-cell content was estimated considering the contribution of the gas in the post-collapse region of the stress–strain curves (effective gas pressure). EBA CC corresponds to foams with low interconnectivity of the cellular structure (around 40%), EBA MO presents an intermediate open-cell content (68%), and finally, there are two types of open-cell foams, EBA OC HT and EBA OC LT both with open-cell contents higher than 95%. The difference between EBA OC HT and EBA OC LT is the level of interconnection in the cellular structure. As the holes in the cell walls are larger in EBA OC LT foams, this open-cell material presents a similar level of interconnection than that of the open-cell PU foam used as a reference. However, as the EBA OC HT foam is produced deforming EBA MO foams, small holes are created in the cell walls restricting the movement of the gas through the cellular structure. As a result, the tortuosity of the EBA OC HT foams is slightly lower than that of EBA MO foams due to the effect of these small holes but much higher than that of EBA OC LT or the PU foams owing to the small size of the holes. These differences in the level of the interconnectivity of the cellular structure can be observed in the SEM micrographs displayed in Figure 2:

Figure 2(a) shows the cellular structure of the closed cell material. As it was explained previously, the level of the interconnectivity of the cellular structure in EBA CC is very low, and in the majority of the cells, the gas is enclosed inside them. Furthermore, the cell size of this material is much lower (266 μm) than that of the rest of the foams. This can be explained, taking into account the nucleation effect and the degeneration mechanisms of the cellular structure. The effect of the degeneration processes on the cellular structure can be correlated to the gel content. High gel-content values are indicative of high viscosity of the polymer

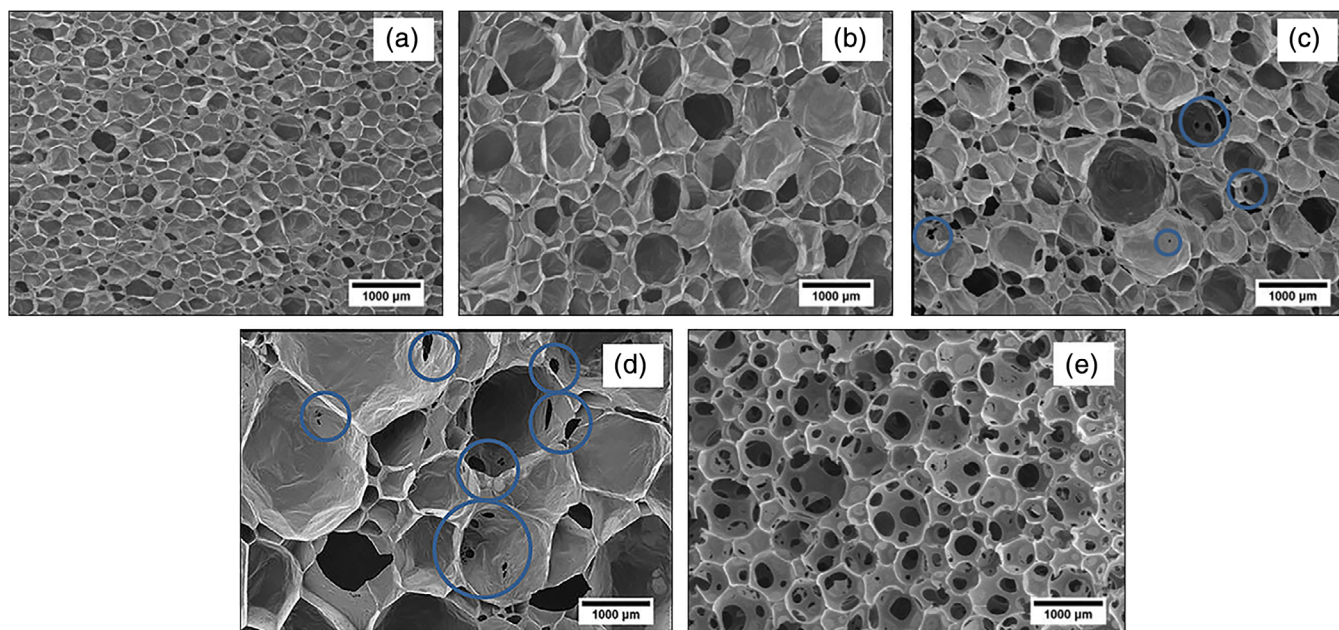


Figure 2. SEM micrographs of the materials under study: (a) EBA CC; (b) EBA MO; (c) EBA OC HT; (d) EBA OC LT and (e) PU used as a reference. [Color figure can be viewed at wileyonlinelibrary.com]

matrix. If the viscosity is high, the degeneration processes are restricted, and thus, cells with lower cell sizes are created. The results show a clear correlation between cell size and gel content; a higher gel-content promotes smaller cell sizes.

The EBA MO foam presents higher cellular structure interconnectivity (68% open-cell content) but far from that observed for both OC HT and OC LT foams [Figure 2(b)]. It is remarkable the effect of the mechanical process performed, aiming at breaking the cell walls. Considering that EBA OC HT foams [Figure 2(c)] with an open-cell content of 95% are obtained from the EBA MO ones, it is clear that the deformation process is very effective to generate open-cell materials.

EBA OC LT foams are characterized by the presence of huge holes in the cell walls. Furthermore, the average cell size of this material is much larger than, for example, the EBA OC HT one (up to 2.67 times larger). As it was mentioned earlier, EBA OC LT [Figure 2(d)] foams are produced directly in the fabrication process. For this purpose, the gas pressure must be able to break the walls during expansion and thus, the viscosity should be low. This low viscosity leads to a side effect, the large cell size. As the viscosity after the crosslinking process is low, the cell walls can be stretched to a higher level resulting in a cellular structure mainly formed by large cells. This is consistent with the low value of the gel content of the OC LT. EBA CC presents the highest gel content level (69%), whereas EBA MO and EBA OC HT have a similar gel content level (between 50% and 60%). In spite of the different level of interconnectivity in MO and OC HT foams, it was expected that both values were similar if it is considered that the EBA OC HT foams were produced from the EBA MO ones. As the foam is already crosslinked before the deformation process necessary to break the cell walls, the crosslinked phase is not affected by this mechanical rupture. Finally, the gel content level of the EBA OC LT is very low (27%).

Another aspect to take into account to explain the difference in cell size, as it was discussed previously, is the degeneration mechanisms of the cellular structure. OC LT materials are prone to suffer from coalescence due to its low viscosity, and this could lead to higher cell sizes.

The densities of the EBA foams are ranged between 20 and 24 kg m⁻³. The materials expanded around 47 times, considering the initial density of the polymer matrix. This density is smaller than that of the PU foam used as a reference. It is also remarkable, the low crystallinity (between 13 and 15%) of the foams regardless of the type of material. The butyl acrylate groups induce a considerable disorder in the ethylene chains, and as a result, the crystallinity is much lower than that of a LDPE polymer.

Physical Properties

Mechanical Properties. The mechanical properties of the foamed materials were tested at low and high strain rates. The strain–stress curves of foamed materials have been deeply analyzed by several authors.^{5,9,14,45–47} The typical stress–strain curve can be divided into three different regions. In the first region, there is a linear dependency between the stress and the strain. Two different mechanisms define this linear region depending on the level of the interconnectivity of the cellular structure: cell edges bending in open-cell materials and cell edges bending and cell walls stretching in closed cell ones. This linear behavior finishes when the stress reaches the collapse stress at a certain strain. At higher strains, a new region, also dependent on the type of cellular structure interconnectivity, starts. In the case of open-cell materials, this region is characterized by the presence of a plateau. However, the contribution of gas inside the cells plays a key role in this region for closed cell materials produced from flexible polymers such as polyolefins. The stress tends to increase due to the compression of the gas inside the cells. Due to this effect, the

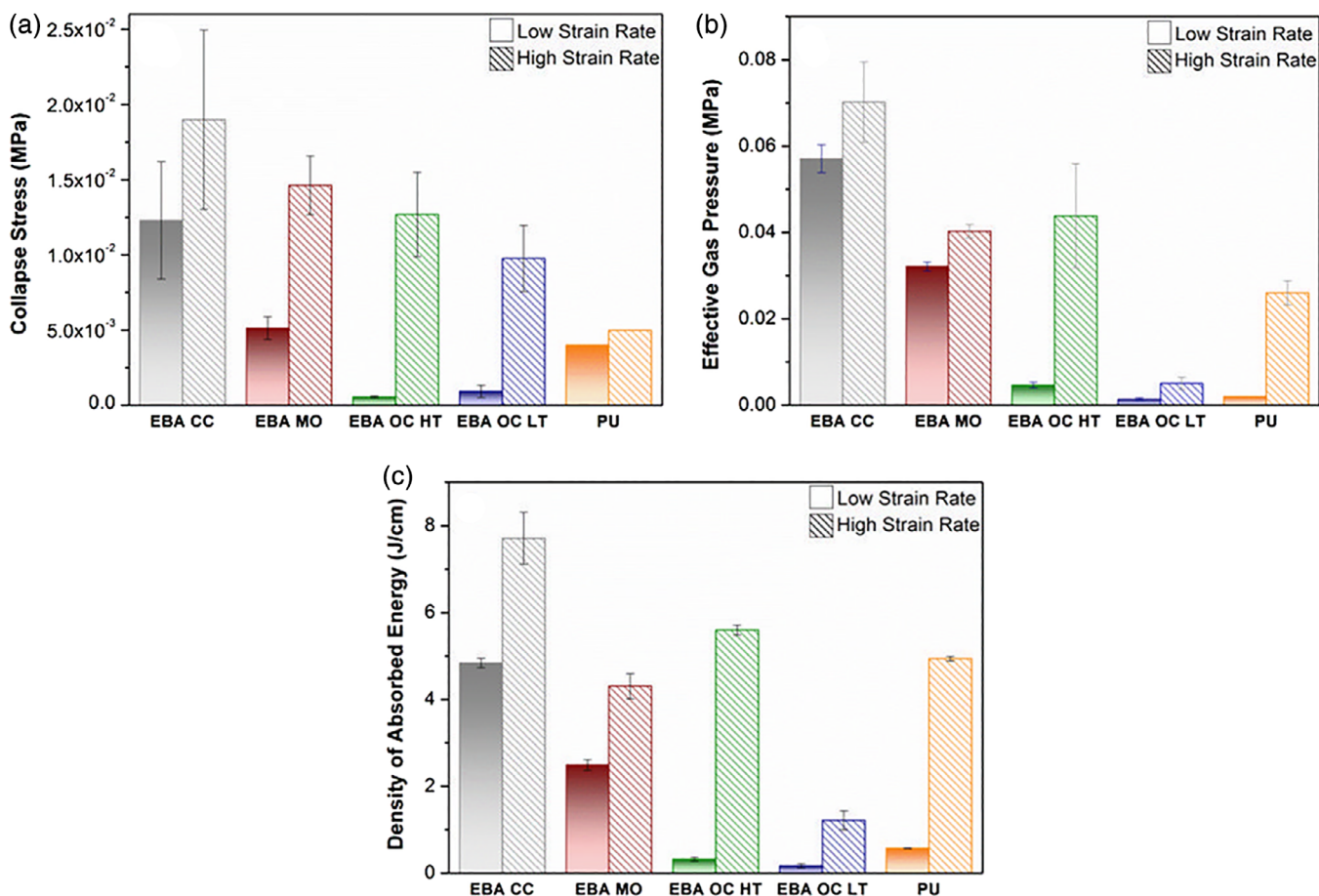


Figure 3. Comparative of the mechanical properties of the different EBA foams and the reference PU at low and high strain rates. (a) Effective gas pressure (MPa); (b) collapse stress (MPa), and (c) density of absorbed energy (J cm^{-3}). [Color figure can be viewed at wileyonlinelibrary.com]

open-cell content can be extracted from these stress–strain curves according to the Gent and Thomas model in this region (strain range between 20 and 60%) (2). Considering this model, a high value of the effective gas pressure (slope) is related to the presence of gas inside the cells (closed cell materials). For open-cell foams, as the gas can escape out of the material at these strains, the value of the effective gas pressure is negligible. Finally, the last region of the stress–strain curves is defined at higher strains ($> 65\%$), when the foam is collapsed, and the upper and lower faces of cells are in contact (densification region). In this region, the stress greatly increases when strain rises.

Three mechanical parameters have been analyzed at both strain rates: the effective gas pressure, the collapse stress, and the density of absorbed energy. This analysis aims at determining

Table II. Percentage of Gas Which Remains in the Sample in the High Strain Compression Tests

Sample	Tortuosity	% gas inside the sample
EBA MO	4.3 ± 0.2	71.4
EBA OC HT	4.0 ± 0.7	69.3
EBA OC LT	1.9 ± 0.2	35.4
PU	1.9 ± 0.1	35.4

whether the cellular structure tortuosity affects the stress–strain curve in the post-collapse region depending on the strain rate.

The main results obtained at both strain rates are compared in Figure 3:

The collapse stress [Figure 3(a)] is clearly influenced by the level of the interconnectivity. This parameter decreases when the level of interconnectivity increases at both low and high strain rates. In all cases, the obtained values at high strain rates are higher than those measured at low strain rates; this is due to the viscoelastic behavior of the polymeric matrix of these foams.

Concerning the effective gas pressure [Figure 3(b)], it can be observed that the contribution of gas is very high for CC and MO regardless of the strain rate. As it was observed previously in the SEM micrographs [Figure 2(a,b)] the level of the interconnectivity of the cellular structure is very low, and thus, it is expected that the gas remains inside the cellular structure in the post-collapse region. Focusing on open-cell foams, both OC HT and OC LT foams behave similarly as the reference open-cell PU foam at low strain rates. The gas has enough time to leave the foam during the compression test, and the curves are characterized by the presence of a plateau at these strains (i.e., a very small slope in the stress–strain curve). Therefore, at low strain rates, the open-cell EBA foams present a similar behavior to that of PU foams.

However, it is remarkable the effect of the strain rate for the OC HT foam. At high strain rates, there is a large contribution of the gas in OC HT foams in the post-collapse region. The effective gas pressure of EBA OC HT foam is very similar to the EBA MO foam. This surprising effect can be explained, taking into account the cellular structure tortuosity.

The mechanical test at high strain rates is up to 500 times faster than at low strain rates. As a consequence, the time that the gas phase has to escape out of the sample is much lower. If the structure is very tortuous, the gas cannot leave the sample in the short time of the impact event (around 12 ms) and therefore remains inside contributing to the detected stress. However, in the case of the EBA OC LT and PU foams, as the tortuosity is half less than that of EBA OC HT foam, a significant amount of gas can escape during the impact test. As a result, EBA OC LT and PU behave as an open-cell foam at both strain rates showing a very small slope in the stress-strain curve in the post-collapse region.

If it is considered that the speed of the gas molecules is the speed of the impact tests (2.3 m s^{-1}) and the test takes place in 12 ms, the distance which the gas molecules can go across can be estimated ($d_1 = 27.6 \text{ mm}$). Considering that the length of the cubic samples is 45 mm, a gas molecule that stays in the middle of the sample must go across 22.5 mm to leave the sample. However, these 22.5 mm is the ideal value, but taking into account the tortuosity of the cellular structure, this distance increases depending on the tortuosity value (4).

$$d_2 = L \cdot T \quad (4)$$

where L is half of the length (22.5 mm) of the cubes used for the mechanical tests (shortest distance), and T is the tortuosity.

The relation between both distances (d_1 and d_2) indicates the percentage of gas which remains inside the sample (Table II).

Up to 70% of the total gas remains inside the foam in EBA MO and EBA OC HT. This is a considerable gas contribution behaving these materials as almost closed cell materials at high strain rates. However, this gas contribution is considerably lower (35%) for the EBA OC LT and the PU materials.

To corroborate the previous statement, the density of absorbed energy was also calculated. Closed cell materials are used for several applications in which high-energy absorptions are required (packaging of different type of items and body protection elements). It is expected that the absorbed energy increases as the level of interconnectivity is reduced. Figure 3(c) displays the main results obtained for the energy absorptions. At low strain rates, it is observed this clear relationship between energy absorption and the level of interconnectivity. The CC and the MO present higher energy absorptions than the open-cell foams. However, it is also confirmed here how the EBA OC HT foam presents a noticeable dependency on the strain rate. At high strain rates, this material can absorb a large amount of energy, very similar to EBA CC and much higher than EBA OC LT. This result is in agreement with that obtained for the effective gas pressure, and therefore, the cellular structure interconnectivity and the tortuosity affects the mechanical properties markedly.

EBA OC HT foams present a defined double behavior depending on the strain rate: they behave as an open-cell foam at low strain

rates and as a closed cell foam at high strain rates. This remarkable effect makes these materials very interesting for applications where comfort and protection are required because this material shows both effects in just one material.

Dynamic Mechanical Behavior and Thermal Expansion

Figure 4 shows the modulus of the complex modulus as a function of temperature for the materials under study. For all the materials, the stiffness decreases when the temperature rises. As it was expected, there is a clear influence of the cellular structure interconnectivity on this parameter. The EBA CC foam presents the highest modulus of the complex modulus in the temperature range between -40 and $40 \text{ }^\circ\text{C}$. In these materials, both cells edge bending, and cell faces stretching contribute to the stiffness of the materials, and due to this, the material presents higher storage modulus.

Furthermore, the relationship between the modulus and the cellular structure interconnectivity is also fulfilled for EBA MO, whose modulus is found between the values of the material with low cellular structure interconnectivity (EBA CC) and the open-cell materials. Open-cell materials have the lowest modulus. The values for both EBA OC HT and EBA OC LT foams are lower than those obtained for the open-cell PU foam at any temperature, which is probably due to the lower density and as consequence higher porosity of the polyolefin-based foams.

$\tan \delta$ is used to determine the ability of a material to damp vibrations. High values of $\tan \delta$ indicate better behavior for damping mechanical vibrations. The results are presented in Figure 5 for temperatures between -40 and $40 \text{ }^\circ\text{C}$. In the range of temperatures under study, no relaxations of the matrix polymer were detected in the $\tan \delta$ curve. For all the materials, the damping factor was almost constant, except for the EBA OC HT that showed an increase.

When EBA CC, EBA MO and the open-cell foams are compared, it is observed that $\tan \delta$ is higher for open-cell foams than for the ones with lower cellular structure interconnectivity. Besides, both EBA OC HT and EBA OC LT present higher $\tan \delta$ than the open-cell PU foam. Therefore, these open-cell EBA foams present a better behavior than the PU foam for damping vibrations. This

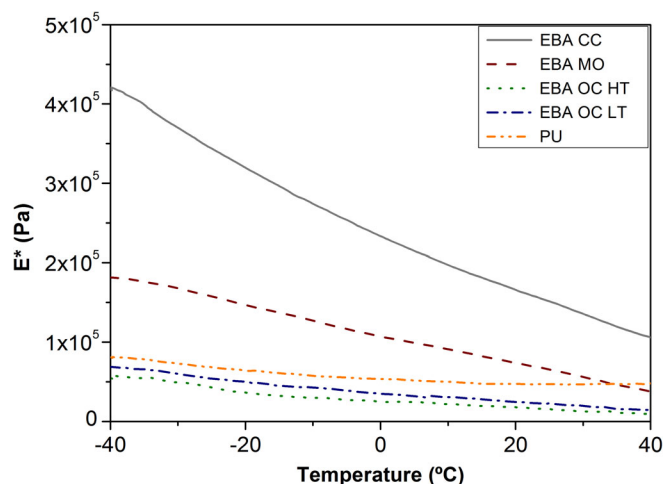


Figure 4. Modulus of the complex modulus (E^*) versus temperature for the materials under study. [Color figure can be viewed at wileyonlinelibrary.com]

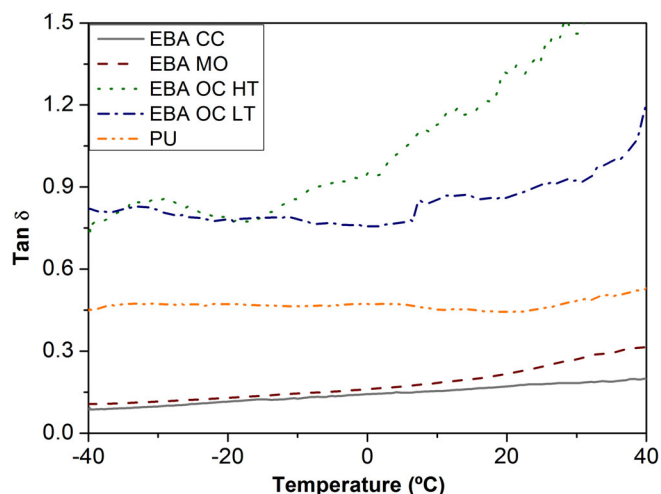


Figure 5. Tan δ versus temperature for the materials under study. [Color figure can be viewed at wileyonlinelibrary.com]

is a remarkable result, showing that apart from the viscoelastic damping coming from the base material, which is the main reason for the values of tan δ found in the EBA CC and EBA MO materials,^{48,49} there is an additional damping mechanism in the open-cell polyolefin foams that allows increasing tan δ values from around 0.2 for the materials with low open-cell contents to 0.9 for the open-cell foam with low tortuosity and to even higher values for the open-cell high tortuous material. This additional damping mechanism should be connected with the energy dissipated by the gas phase when moves outside and inside the sample during the mechanical cycle. From a practical point of view, this new behavior opens the possibility of using these new foams as very efficient materials for damping mechanical vibrations.

Once the viscoelastic behavior has been characterized, the thermal stability of the materials was also considered.

To quantify this property, the temperature to reduce the thickness of the foam by 10% was measured. The values are displayed in Table III:

It is observed in Table III, that this temperature decreases as the level of interconnectivity increases, being the EBA CC the most thermally stable material, whereas the collapse of the open-cell foams starts at a temperature below 70 °C.

Acoustic Properties

The acoustic absorption of the materials under study is shown in Figure 6.

Table III. Temperature to Reduce the Thickness of the Foam by 10%

Sample	Temperature (°C)
EBA CC	83.6 ± 5.2
EBA MO	80.5 ± 0.6
EBA OC HT	68.7 ± 1.3
EBA OC LT	68.2 ± 2.8
PU	- ^a

^a The thickness of the PU foam is not reduced in this temperature range.

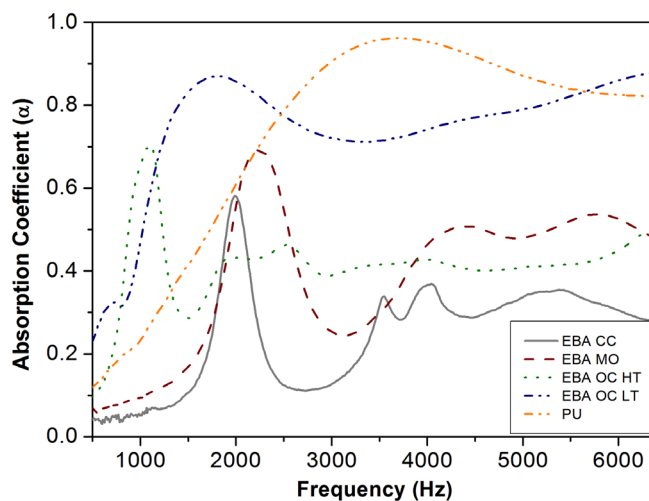


Figure 6. Absorption coefficient versus frequency of the materials under study. [Color figure can be viewed at wileyonlinelibrary.com]

It can be observed a clear influence of the cellular structure interconnectivity on the absorption coefficient (α). The EBA CC foam displays the lower absorptions far from those obtained for any of the open-cell foams. The EBA OC LT presents higher absorptions than that obtained for the EBA OC HT one in all frequency range. A possible explanation of this result can be based on how the sound waves are propagated through the cellular structure. As the holes are larger in EBA OC LT foams, the waves can propagate more easily than through tiny holes. As a result, it can be stated that EBA OC LT foams are more suitable for acoustic absorption than the EBA OC HT ones. It can also be outlined that the EBA OC LT foam shows high values of the acoustic absorption, in the same range than those found for the open-cell PU foam, typically used for acoustic absorption.

Setting aside the cellular structure interconnectivity, all EBA foams display an interesting feature: the maximum absorptions for the EBA cellular polymers appear at lower frequencies than those of the PU foam. Aiming at understanding better these results, the normalized absorption coefficient (α_n) has been calculated by using the following eq. (5):

$$\alpha_n = \frac{\int_{f_1}^{f_2} \alpha(f) df}{f_2 - f_1} \quad (5)$$

where f_2 and f_1 are the frequencies used as limits in the integration.

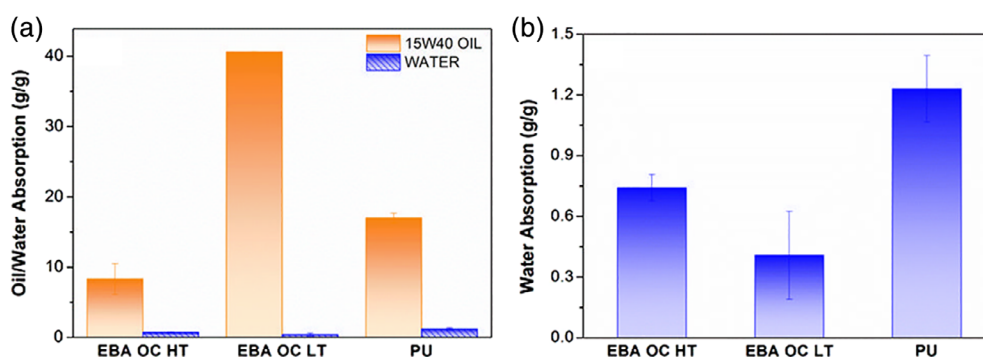
The results are summarized in Table IV, where the frequency of the peak in the acoustic absorption curve, the normalized absorption coefficient in the whole frequency ranges (500–6400 Hz) and the normalized absorption coefficient at low frequencies (500–2500 Hz) are collected:

As it was emphasized previously, there is a considerable difference in the frequency of the maximum peaks for the EBA-based foams (below 2500 Hz) and the PU foam used as a reference (above 3500 Hz).

Concerning the normalized absorption coefficient, it can be observed how this parameter is affected by the tortuosity. As it

Table IV. Frequency of the Maximum in the Acoustic Absorption Curve, Normalized Absorption Coefficients in the Whole Frequency Range and Normalized Absorption Coefficients at Low Frequencies

Samples	Frequency Maximum (Hz)	α_n (500–6400 Hz)	α_n (500–2500 Hz)
EBA CC	1992 ± 60	0.24 ± 0.03	0.18 ± 0.01
EBA MO	2240 ± 169	0.39 ± 0.03	0.29 ± 0.04
EBA OC HT	1048 ± 112	0.41 ± 0.07	0.40 ± 0.07
EBA OC LT	1684 ± 275	0.74 ± 0.07	0.68 ± 0.12
PU	3715 ± 106	0.73 ± 0.00	0.43 ± 0.01

**Figure 7.** (a) Comparative between oil (motor oil 15W40) and water absorptions and (b) water absorptions of the open-cell foams under study. [Color figure can be viewed at wileyonlinelibrary.com]

was expected, the EBA CC foam has the poorest acoustic absorption. There is a slight difference (0.02) in absorption between the MO and OC HT foam. Despite creating holes in the cell walls, it seems that this fact has not any considerable effect on the acoustic absorption if the acoustic absorption is evaluated in the whole frequency range. However, this difference is wider at low frequencies (0.11). Focusing the analysis on the tortuosity, it can be inferred from the data of Table IV, that the tortuosity plays a key role on this property, being the absorption of the EBA OC LT much higher than that of EBA OC HT foam. It is also remarkable that the EBA OC LT (0.74) presents similar acoustic absorptions to the open-cell PU foam (0.73). Particularly, EBA OC LT shows the highest absorption coefficient (0.68) at low frequencies, whereas the PU foam has a poorer performance in this range (0.43).

These results indicate the extremely good acoustic absorption of the EBA OC LT foam, standing out the excellent absorptions at low frequencies, which makes this material a potential alternative to the current materials used for acoustic absorption.

Oil Absorption

The oil (commercial motor oil 15W40) and the water absorption capacities of the open-cell EBA foams have been measured and

have been compared to the reference PU foam. The oil absorption of the EBA CC and the EBA MO foams was not measured. The oil cannot penetrate in the cellular structure of these materials due to the lack of interconnectivity of the cellular structure.

The oil and water absorptions of the foams under study are shown and compared in Figure 7.

From Figure 7, it can be inferred that the affinity toward oil in all the materials is much higher than the hydrophilic behavior. Furthermore, the cellular structure tortuosity plays once again a critical role. The oil absorption of the EBA OC LT foam is nearly five times higher than that of the EBA OC HT one. It is also noteworthy that the EBA OC LT presents better oil absorptions than the PU foam characterized in this article. Here, it is convenient to clarify that there are other examples in the literature based on studies of oil absorption of open-cell PU foams, which have oil absorptions up to 60 g of oil per gram of foam.²⁷ Nevertheless, considering that any additional surface treatments have been performed in the EBA foams, 40 g of oil per gram of foam can be considered a significant oil uptake.

Concerning the water absorptions, both open-cell EBA foams are more hydrophobic than the PU foam. Water absorptions, as low as 0.40 g of water per gram of foam, were obtained without

Table V. Non-Recovered Deformation (NRD) values of EBA OC LT and the PU Foam as a Function of the Compressive Cycle

Sample	NRD % (1st cycle)	NRD % (5th cycle)	NRD % (10th cycle)	NRD % (15th cycle)	NRD % (20th cycle)
EBA OC LT	0.1	2.1	3.1	3.1	4.1
PU	0.2	1.1	2.0	2.0	2.0

performing any surface treatment. This result constitutes a relevant benefit in comparison with PU foams.

Another aspect of being considered is the reusability of the materials, which is a critical requirement for a material to be used for this application. As a consequence, the material must be employed as many times as necessary without losing performance. For this purpose, the EBA OC LT foam and the open-cell PU foam were subjected to 20 compressive cycles.⁵⁰ The parameter to be analyzed in the reusability tests is called the non-recovered deformation (NRD). This parameter should be as low as possible and constant along the consecutive cycles to consider a material as reusable.

The non-recovered deformations values for the two analyzed materials are exposed in Table V:

Both materials present an almost constant behavior along the cycles. The non-recovered deformation slightly increases from the first to the last cycle in both materials.

Furthermore, both materials have non-recovered deformation values under 5%, which means that these materials recover almost completely after compression. This result was expected for the PU because it is used for applications in which the total recovery of the material is required (comfort). Thus, it can be observed in Table V that the EBA OC LT foam nearly reproduces the performance of open-cell PU foams.

CONCLUSIONS

The physical properties of novel crosslinked EBA foams with different cellular structure interconnectivity and tortuosities have been analyzed and compared with those obtained for an open-cell PU foam used as a reference.

Concerning the mechanical properties, it has been determined that the cellular structure tortuosity has a critical influence depending on the strain rate of deformation. On the one hand, the low tortuous foams behave as an open-cell foam at both low and high strain rates. On the other hand, the contribution of gas increases dramatically at high strain rates for the high tortuous foam, behaving this foam similarly to a closed cell foam at high strains. The small size and the small amount of the holes in the high tortuous foams allow the escape of the gas at low strain rates, but at high strain rates, the gas does not have enough time to escape through the tiny holes. As a result, there is a marked dependence of the foam behavior with the strain rate.

The low tortuous foams present excellent sound absorptions in the whole range of frequencies, but it is remarkable its superior absorption at low frequencies in a region where the open-cell PU foam has a poorer performance. In addition, the cellular structure tortuosity plays a critical role on the sound absorption, being low tortuous foams much better absorbers than the high tortuous ones, because the sound waves can penetrate easily through larger holes.

The effect of the cellular structure tortuosity on the oil absorption has been analyzed, concluding that the oil can penetrate easily through the large holes of the low tortuous foams. It is also noteworthy that these EBA-based foams can be reused at least 20 times.

Furthermore, these open-cell EBA foams are suitable for damping vibrations due to its high $\tan \delta$ value.

As a summary of this research, we can conclude that these novel open-cell EBA foams can be considered as a potential alternative to open-cell PU foams for several applications.

ACKNOWLEDGMENTS

This work performed with the financial support from DI grant DI-15-07952 (E. Lopez-Gonzalez) from the Spanish Ministry of Economy, Industry, and Competitiveness. Financial assistance from MINECO, FEDER, UE (MAT2015-69234-R) and the Junte of Castile and Leon (VA275P18) are gratefully acknowledged.

REFERENCES

1. Reducing Marine Litter: action on single-use plastics and fishing gear. European Commission.
2. Mills, N. *Polymer Foams Handbook*; Elsevier Science Publishers: Amsterdam, **2007**.
3. Lee, S. T.; Ramesh, N. S., Eds. *Polymeric Foams: Mechanisms and Materials*; CRC Press Taylor & Francis Group: Boca Raton, **2004**.
4. Gibson, L. J.; Ashby, M. F. In *Cellular Solid: Structure and Properties*; Clarke, D. R.; Suresh, S.; Ward, I. M., Eds., 2nd ed. Cambridge University Press: Cambridge, U.K., **1997**.
5. Rodriguez-Perez, M. A. *Adv. Polym. Sci.* **2005**, *184*, 97.
6. Nagy, A.; Ko, W. L.; Lindholm, U. S. *J. Cell. Plast.* **1974**, *10*, 127.
7. Avella, M.; Cocca, M.; Errico, M. E.; Gentile, G. *J. Cell. Plast.* **2011**, *47*, 271.
8. Mills, N. J.; Fitzgerald, C.; Gilchrist, A.; Verdejo, R. *Compos. Sci. Technol.* **2003**, *63*, 2389.
9. Verdejo, R.; Mills, N. J. *J. Biomech.* **2004**, *37*, 1379.
10. Mosanenzadeh, S. G.; Naguib, H. E.; Park, C. B.; Atalla, N. *Polym. Eng. Sci.* **2013**, *53*, 1979.
11. Chen, S. M.; Jiang, Y. *Polym. Compos.* **2018**, *39*, 1370.
12. Klempner, D.; Sendjarevic, V., Eds. *Handbook of Polymeric Foams and Foam Technology*; Hanser Publishers: Munich, **1991**.
13. Rodriguez-Perez, M. A.; Velasco, J. I.; Arencon, D.; Almanza, O.; de Saja, J. A. *J. Appl. Polym. Sci.* **1999**, *75*, 156.
14. Zhu, H. X.; Knott, J. F.; Mills, N. J. *J. Mech. Phys. Solids.* **1997**, *45*, 319-327-343.
15. DesMarais, T.A. U.S. Pat. 4067832A (**1978**).
16. Radovich, D.A.; Lowery, M.K. U.S. Pat.4546122A (**1985**).
17. Leenslag, J.W.; Cunningham, A.; Eling, B. U.S. Pat. 5900442A (**1999**).
18. Scarpa, F.; Pastorino, P.; Garelli, A.; Patsias, S.; Ruzzene, M. *Phys. Status SolidiB.* **2005**, *242*, 681.
19. Gwon, J. G.; Kim, S. K.; Kim, J. H. *Des. Mater.* **2016**, *53*, 448.
20. Peterson, C. H. *Adv. Mar. Biol.* **2001**, *39*, 1.
21. Skalski, J. R.; Coats, D. A.; Fukuyama, A. K. *Environ. Manag.* **2001**, *28*, 9.

22. Adebajo, M. O.; Frost, R. L.; Klopogge, J. T.; Carmody, O.; Kokot, S. *J. Porous. Mater.* **2003**, *10*, 159.
23. Calcagnile, P.; Fragouli, D.; Bayer, I. S.; Anyfantis, G. C.; Martiradonn, L.; Cozzoli, P. D.; Cingolani, R.; Athanassiou, A. *ACS Nano.* **2012**, *6*, 5413.
24. Pinto, J.; Athanassiou, A.; Fragouli, D. *J. Phys. D Appl. Phys.* **2016**, *49*, 145601.
25. Wang, P.; Zou, C.; Zhong, H. *Adv. Mater. Res.* **2012**, *518*, 847.
26. Thakur, S.; Jahid, M. A.; Hu, J. *Polym. Int.* **2018**, *67*, 1386.
27. Pinto, J.; Heredia-Guerrero, J. A.; Athanassiou, A.; Fragouli, D. *Int. J. Environ. Sci. Technol.* **2017**, *14*, 2055. <https://doi.org/10.1007/s13762-017-1310-6>.
28. Wang, C. F.; Lin, S. J. *ACS Appl. Mater. Inter.* **2013**, *5*, 8861.
29. Zhu, Q.; Chu, Y.; Wang, Z.; Chen, N.; Lin, L.; Liu, F.; Pan, Q. *J. Mater. Chem. A.* **2013**, *1*, 5386.
30. Alvarez-Lainez, M.; Rodriguez-Perez, M. A.; de Saja, J. A. *Mater. Lett.* **2014**, *121*, 26.
31. Alvarez-Lainez, M.; Rodriguez-Perez, M. A.; de Saja, J. A. *J. Polym. Sci. Pol. Phys.* **2008**, *46*, 212.
32. Almanza, O.; Rodriguez-Perez, M. A.; de Saja, J. A. *Polym. Int.* **2004**, *53*, 2038.
33. Zhou, H.; Wang, Z.; Xu, G.; Wang, X.; Wen, B.; Jin, S. *Cell. Polym.* **2017**, *37*, 167.
34. Ouassim, H.; Mighri, F.; Rodrigue, D. *Cell. Polym.* **2018**, *37*, 153.
35. Bear, J. *Dynamics of Fluids in Porous Media*; American Elsevier Pub. Co: New York, NY, **1972**.
36. Pfretzschner, J.; Rodriguez, R. M. *Polym. Test.* **1999**, *18*, 81.
37. Mills, N. J.; Zhu, H. X. *J. Mech. Phys. Solids.* **1999**, *47*, 669.
38. Mills, N. J.; Rodriguez-Perez, M. A. *Cell. Polym.* **2001**, *20*, 79.
39. Wang, B.; Wang, M.; Xing, Z.; Zeng, H.; Wu, G. J. *Appl. Polym. Sci.* **2013**, *127*, 912.
40. Eaves, D., Ed. *Handbook of Polymer Foams*; Rapra Technology Limited: Shawbury, **2004**.
41. Pinto, J.; Solorzano, E.; Rodriguez-Perez, M. A. *J. Cell. Plast.* **2013**, *49*, 555.
42. Ruiz-Herrero, J. L.; Rodriguez-Perez, M. A.; de Saja, J. A. *Polym. Test.* **2005**, *24*, 641.
43. Gent, A. N.; Thomas, A. G. *Rubber. Chem. Technol.* **1963**, *36*, 597.
44. Rodriguez-Perez, M. A.; Hidalgo, F.; Solorzano, E.; de Saja, J. A. *Polym. Test.* **2009**, *28*, 188.
45. Menges, G.; Knipschild, F. *Polym. Eng. Sci.* **1975**, *15*, 623.
46. Maiti, S. K.; Gibson, L. J.; Ashby, M. F. *Acta. Metall. Mater.* **1984**, *32*, 1963.
47. Iannace, F.; Iannace, S.; Caprino, G.; Nicolais, L. *Polym. Test.* **2001**, *20*, 643.
48. Rodriguez-Perez, M. A.; de Saja, J. A. *Polym. Test.* **1999**, *19*, 831.
49. Rodriguez-Perez, M. A.; Rodriguez-Llorente, S.; de Saja, J. A. *Polym. Eng. Sci.* **1997**, *39*, 959.
50. Rizvi, A.; Chu, R. K. M.; Lee, J. H.; Park, C. B. *ACS Appl. Mater. Inter.* **2014**, *6*, 21131.